Supplementary Figure 1: Calibration of selective electronic and nuclear inversions

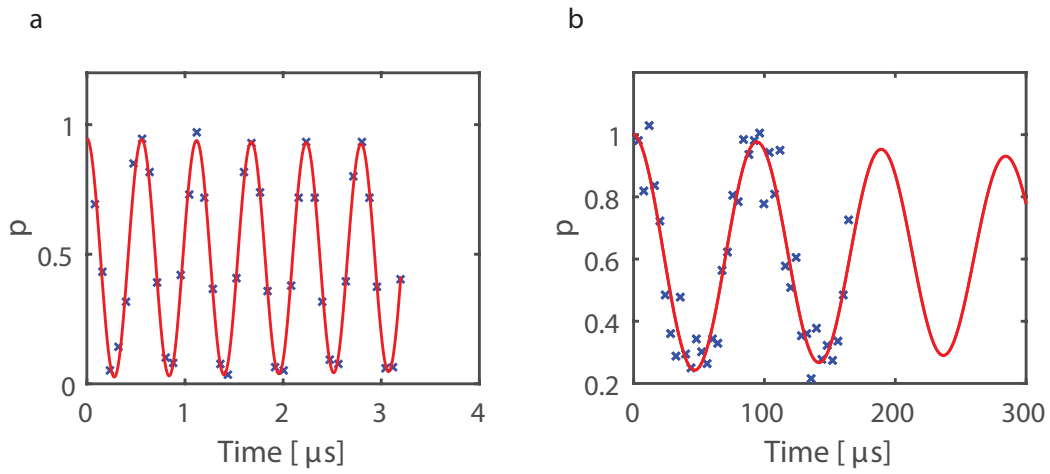

FIG. S1. Calibration of selective Rabi oscillations of (a) the electronic spin and (b) the nuclear spin. The vertical scale is normalized to the maximum possible excursion from a separate calibration measurement. For this NV center, the inversion efficiency was 92% for the electronic spin and 77% for the ^{15}N nuclear spin, respectively. Other NV centers had inversion efficiencies of >90% for the electronic spin and 60-80% for the ^{15}N nuclear spin, respectively. The efficiency for the electronic spin inversion is limited by spurious excitation of the other hyperfine resonance, while the efficiency of the nuclear spin inversion is limited by a combination of NV charge conversion[S1] and imperfections of the rf pulse.

Supplementary Figure 2: Storage and retrieval of electronic Rabi oscillation

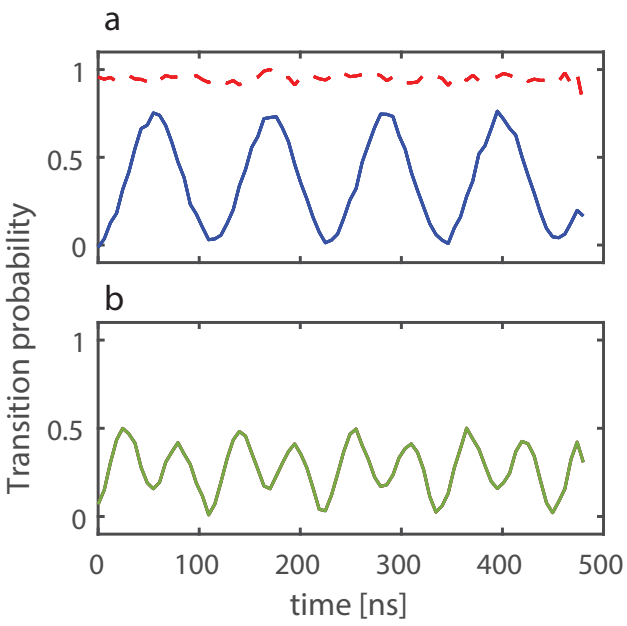

FIG. S2. Test example of the nuclear quantum memory. (a) Measurement to test the store and retrieve operations for the nuclear memory. A Rabi oscillation is performed on the electron spin. The polarization is then transferred to the nuclear spin and the electron spin re-initialized by a laser pulse to clear. The information is then retrieved and read out. The blue curve shows the recovered signal. The dotted red curve shows a control measurement without nuclear memory to verify that the re-initialization clears all information on the electronic spin. The efficiency of the combined store and retrieve operation is only $\sim 70\%$ in this case, because the laser pulse can induce conversion between the NV^- and neutral NV^0 charge states[S1]. To avoid this effect, no laser pules were used during the main correlation sequence presented in Fig. 2 of the main manuscript. (b) Measurement to test the correlation protocol. After an initial Rabi rotation, the state of the electron is stored in the nuclear spin, the electronic spin re-initialized, and the state retrieved. Then, a second identical Rabi rotation is performed before readout. An oscillation with twice the frequency is observed, as expected. The apparent beating is due to the reduced efficiency caused by the laser pulse used for re-initialization.

Supplementary Figure 3: Repetitive readout of nuclear spin state

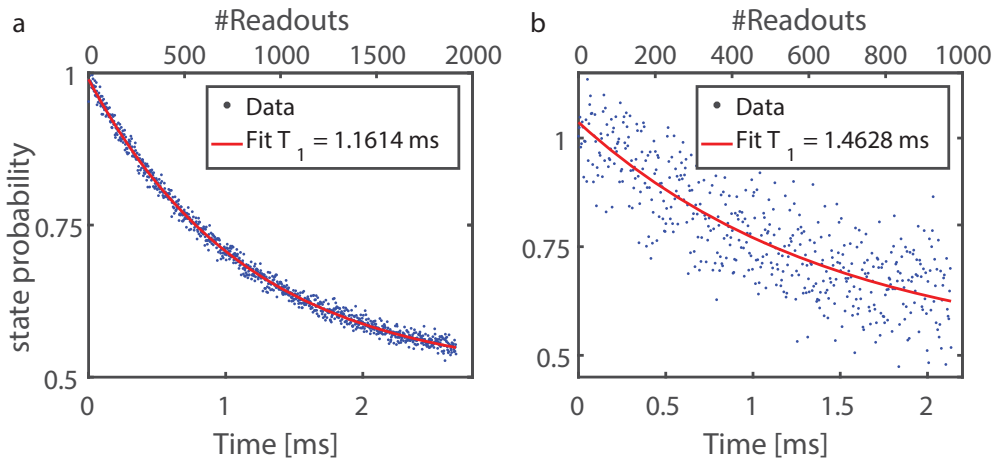

FIG. S3. Repetitive readout of the nuclear spin state is performed to enhance the readout efficiency[S2,S3]. Graphs show the state probability of the nuclear spin after a certain number of readouts n are performed (see dotted box in Fig. 2 in the main manuscripts). (a) is for a bias field of $\sim 350\,\mathrm{mT}$ and (b) for a bias field of $\sim 250\,\mathrm{mT}$.

Supplementary Figure 4: Additional ac sensing plots

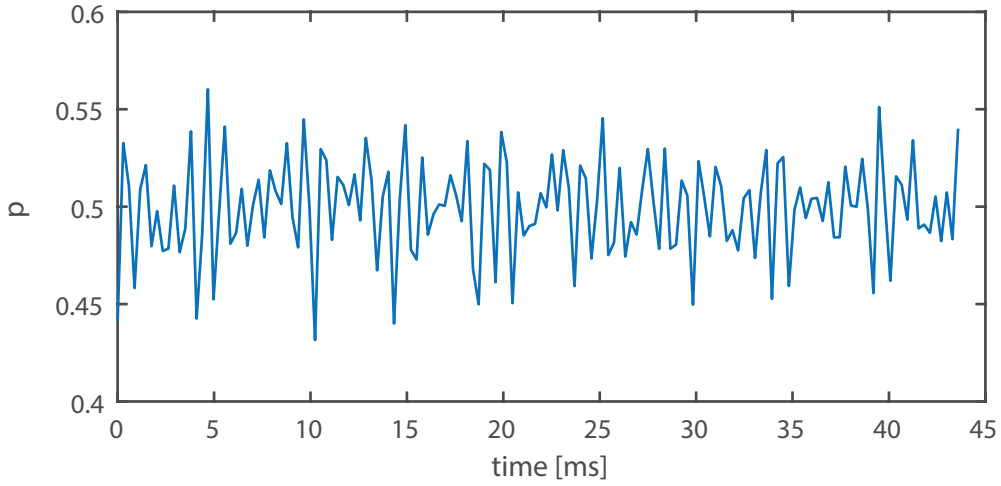

FIG. S4. Time trace for the spectrum presented in Fig. 3(d) in the main manuscript. The beating due to the two frequency components can be nicely seen.

Supplementary Figure 5: Tracking of magnetic field drifts

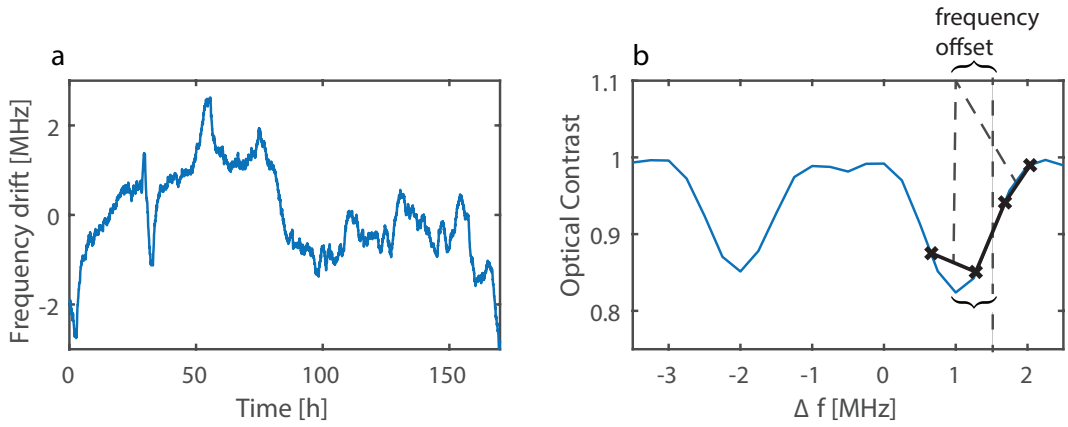

FIG. S5. (a) Relative frequency of the EPR resonance of the NV center over a long measurement period. The standard deviation of point-to-point differences is 33 kHz, corresponding to an uncertainty in magnetic field of 1.2 μT and an uncertainty in the ^{13}C resonance of about 13 Hz. (b) Protocol used to estimate the EPR frequency: A four-point measurement of one hyperfine transition is performed to determine the peak position. A simple tracking algorithm is implemented to follow the EPR peak as it shifts around due to magnetic field drifts. The blue curve shows a representative EPR spectrum with both hyperfine lines, and the crosses indicate representative measurement points.

Supplementary Figure 6: Simulation of ^{13}C NMR linewidth: Contribution by the NV-^{13}C hyperfine coupling

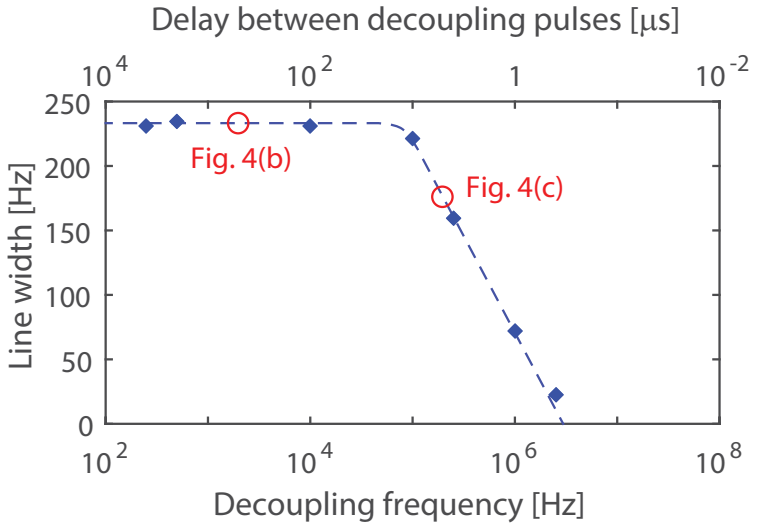

FIG. S6. Simulation of the spectral line width of the ^{13}C NMR resonance with increasing number of decoupling pulses. Only the $m_S = 0 \leftrightarrow -1$ transition is taken into account. Magnetic field, hyperfine parameters and T_1 are set according to the experiment. The simulation demonstrates that a line narrowing can be expected once the decoupling frequency, given by the inverse of the delay time between decoupling pulses, exceeds the hyperfine coupling (here $|a_\parallel| \approx 2\pi \times 140\,\mathrm{kHz}$, see main text). Simulations use the density matrix method[S4], T_1 decay is implemented by stochastic spin flips, and the obtained time traces are processed the same way as the experimental data. Dots are fits to simulated spectra and the dashed line is a guide to the eye. Red open circles indicate the approximate conditions for the spectra of Fig. 4(b) and (c) in the main manuscript, respectively.

Supplementary Figure 7: Simulation of ^{13}C NMR linewidth: Contribution by ^{13}C -^{13}C dipolar couplings

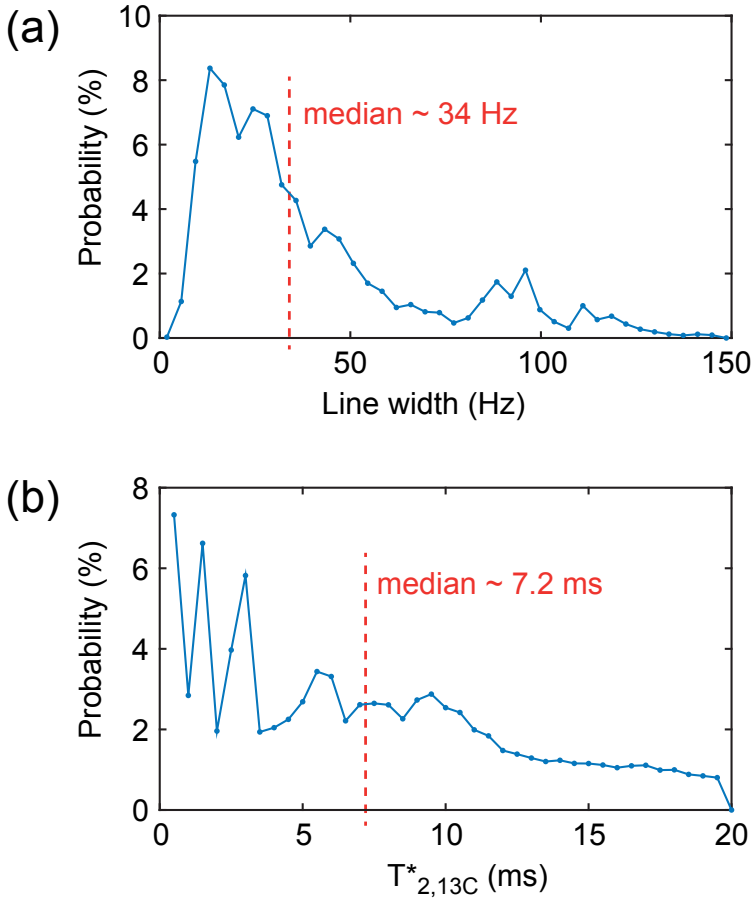

FIG. S7. Histogram of the expected ^{13}C linewidth (a) and the expected ^{13}C dephasing time $T^*_{2,^{13}\mathrm{C}}$ due to ^{13}C -^{13}C couplings. Linewidth is the full width at half maximum of the power spectrum and can be directly compared to the linewidth reported in Fig. 4 of the main manuscript. The linewidth is $\sqrt{2}/(2\pi)$ of the square root of the van Vleck second moment [Ref. S5, p.79, Eq. (3.53)]. The ^{13}C dephasing time $T^*_{2,^{13}\mathrm{C}}$ is $\sqrt{\log 2}/(\pi\times\text{linewidth}) \approx 0.8326/(\pi\times\text{linewidth})$. The histogram was accumulated over 30'000 random configurations of a diamond lattice of $13 \times 13 \times 13$ unit cells and a ^{13}C concentration of 1.07%. The median linewidth predicted by the simulation is 34 Hz, which is significantly smaller than the linewidths observed in the experiments in Fig. 4.

[S1] Aslam, N., Waldherr, G., Neumann, P., Jelezko, F. & Wrachtrup, J. Photo-induced ionization dynamics of the nitrogen vacancy defect in diamond investigated by single-shot charge state detection. *New Journal Of Physics* **15**, 013064 (2013).

[S2] Jiang, L. *et al.* Repetitive readout of a single electronic spin via quantum logic with nuclear spin ancillae. *Science* **326**, 267–272 (2009).

[S3] Neumann, P. *et al.* Single-shot readout of a single nuclear spin. *Science* **329**, 542–544 (2010).

[S4] Boss, J. M. *et al.* One- and two-dimensional nuclear magnetic resonance spectroscopy with a diamond quantum sensor. *Phys. Rev. Lett.* **116**, 197601 (2016).

[S5] Slichter, C. P. *Principles of Magnetic Resonance, 3rd edition* (Springer, Berlin, 1990).